Figures and figure supplements

TPL2 kinase activity regulates microglial inflammatory responses and promotes neurodegeneration in tauopathy mice

Yuanyuan Wang *et al*.

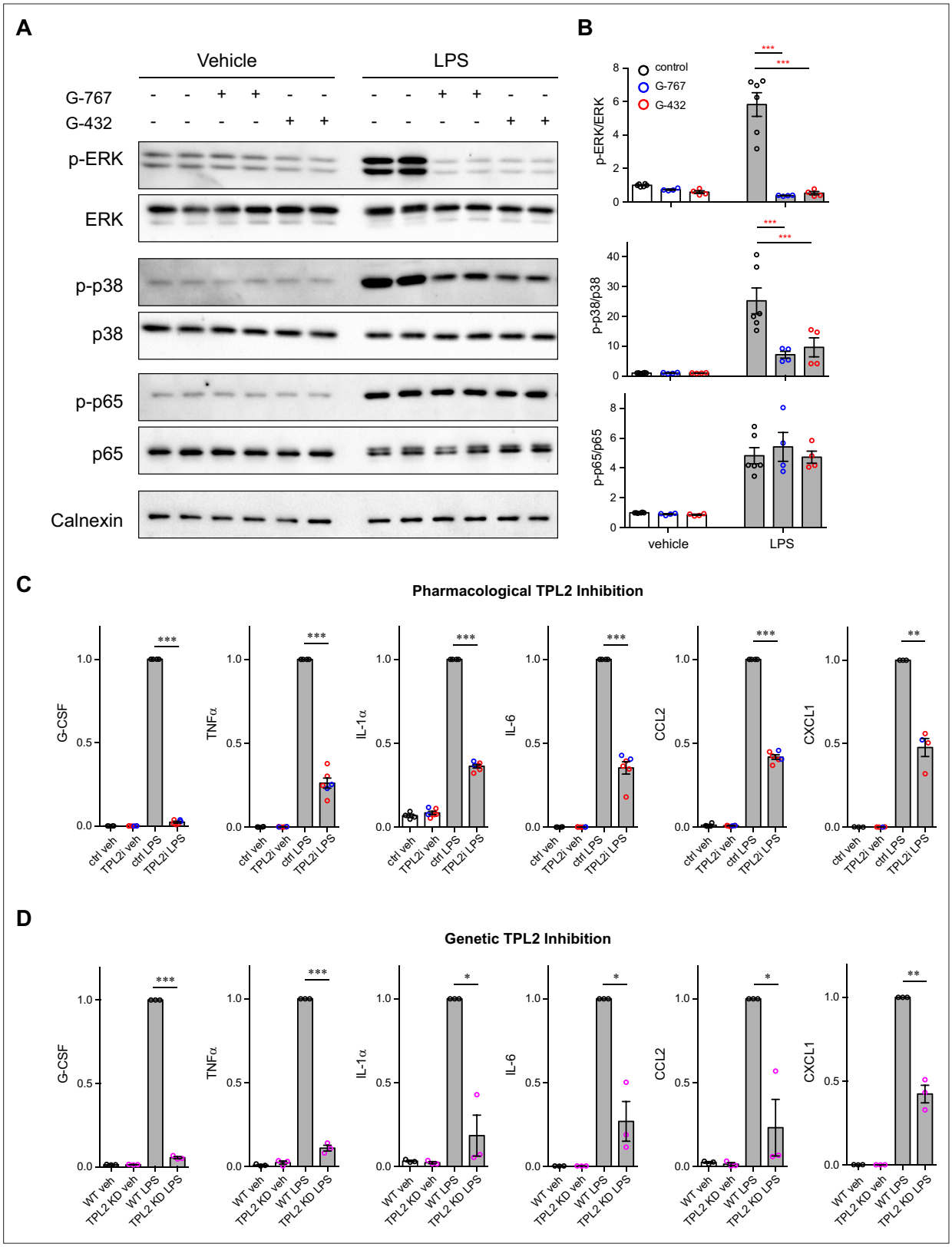

Figure 1. Tumor progression locus 2 (TPL2) modulates mitogen-activated protein kinase (MAPK) signaling and cytokine production by microglia. (**A**) Representative western blots of phospho-ERK, total ERK, phospho-p38, total p38, phospho-p65, total p65, and calnexin (loading control) in lysates from primary microglia cultures treated with vehicle or lipopolysaccharide (LPS) with or without TPL2 inhibitors (2 μM). (**B**) Quantification of western blot data as shown in (**A**). Phosphorylated proteins were first normalized to the corresponding total proteins, and then the normalized values were plotted relative

Figure 1 continued on next page

Figure 1 continued

to the average values from control samples (no LPS, no TPL2 inhibitor) n=4–6. Data are represented by mean ± SEM. ***, p<0.001, two-way ANOVA with Tukey's multiple comparisons test. (**C** and **D**) Quantification of cytokine measurements from the supernatants of WT primary microglia with or without TPL2 inhibitor (**C**) or microglia isolated from WT mice or TPL2 kinase dead (TPL2-KD) mice (**D**) under control or LPS induction (24 hr incubation) conditions. Cytokines highlighted here were selected based on significant LPS induction that was reduced by TPL2 inhibition (pharmacological or genetic) by >50%. Additional cytokine measurements are provided in ***Figure 1—figure supplement 3***. Cytokine measurements were normalized to average values of WT microglia treated with LPS. Data from TPL2 inhibitor G-432 (red circle) and G-767 (blue circle) were combined in (C), n=4–6. n=3 for (**d**). Data are represented by mean ± SEM. *, p<0.05, **, p<0.01, ***, p<0.001, one-way ANOVA with Tukey's multiple comparisons test.

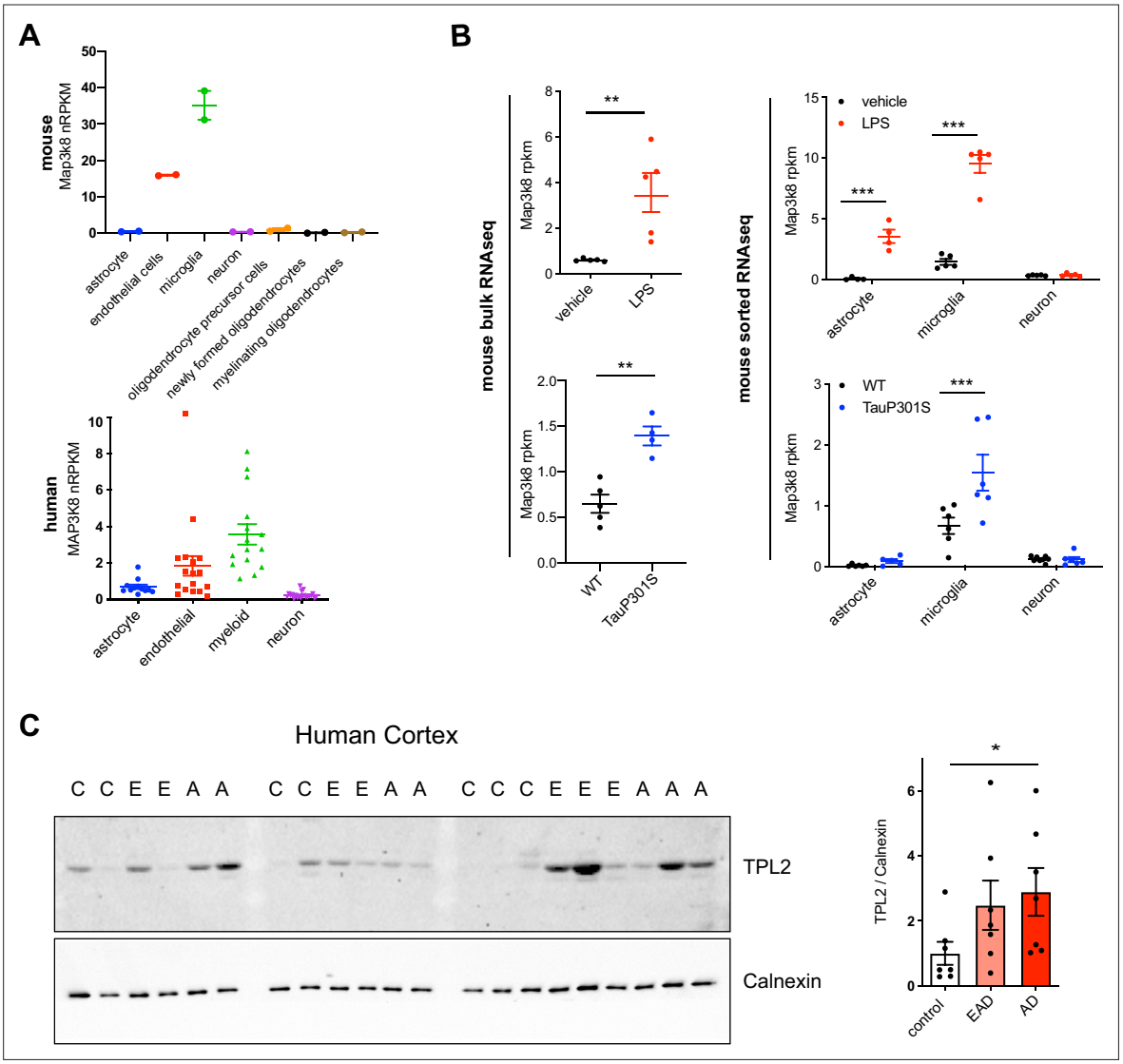

Figure 1—figure supplement 1. Tumor progression locus 2 (TPL2) is upregulated in tauopathy mice and Alzheimer's disease (AD) patients. (**A**) Expression of TPL2 (Map3k8) in various cell types, as indicated, sorted from mouse brain tissue (***Zhang et al., 2014***) (top) or human brain tissue (***Srinivasan et al., 2020***) (bottom). (**B**) Expression of TPL2 in brain bulk tissue (top left; GSE196401) or sorted astrocytes, microglia, and neurons (top right, ***Srinivasan et al., 2016***) from WT mice injected with phosphate-buffered saline (PBS) or lipopolysaccharide (LPS) (10 mg/kg). n=4–5. Expression of TPL2 was also examined in hippocampal bulk tissue (bottom left; GSE186414) or sorted astrocytes, microglia, and neurons (bottom right, ***Friedman et al., 2018*** from hippocampi of WT and TauP301S mice. (**C**) Western blot image and quantification of TPL2 and calnexin as a loading control in lysates from human superior frontal gyrus of healthy control (**C**), early AD (E or EAD) and AD (A or AD) patient brains. TPL2 protein levels were normalized to the average control level after normalization to calnexin. Data are represented by mean ± SEM. *, p<0.05, two-tailed Student's t-test.

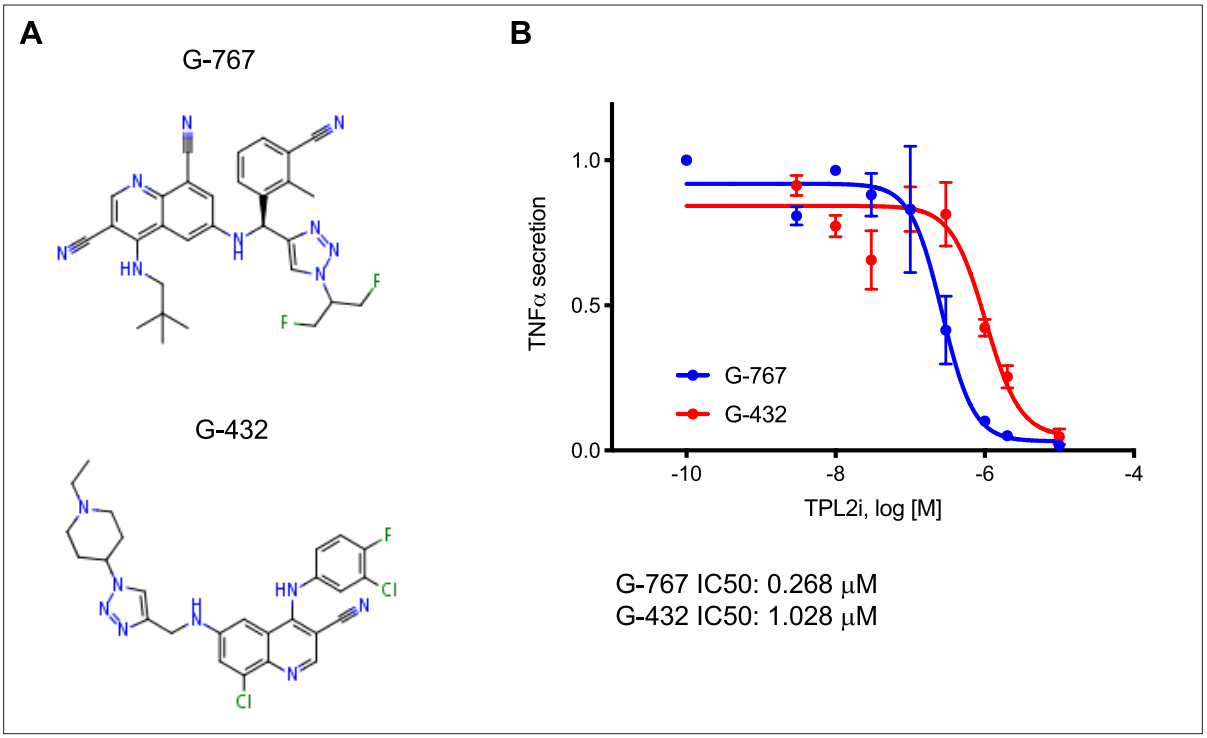

Figure 1—figure supplement 2. Tumor progression locus 2 (TPL2) inhibitor structures and potency dose-response curves. (**A**) Structures of TPL2 inhibitors G-432 and G-767. (**B**) Inhibition dose-response curve of TPL2 inhibitor G-432 or G-767. Measurements were done with primary microglia cultures stimulated with lipopolysaccharide (LPS), using TNFα levels in the cell culture supernatants as the readout. TNFα levels were normalized to average values of microglia treated with LPS, without inhibitor.

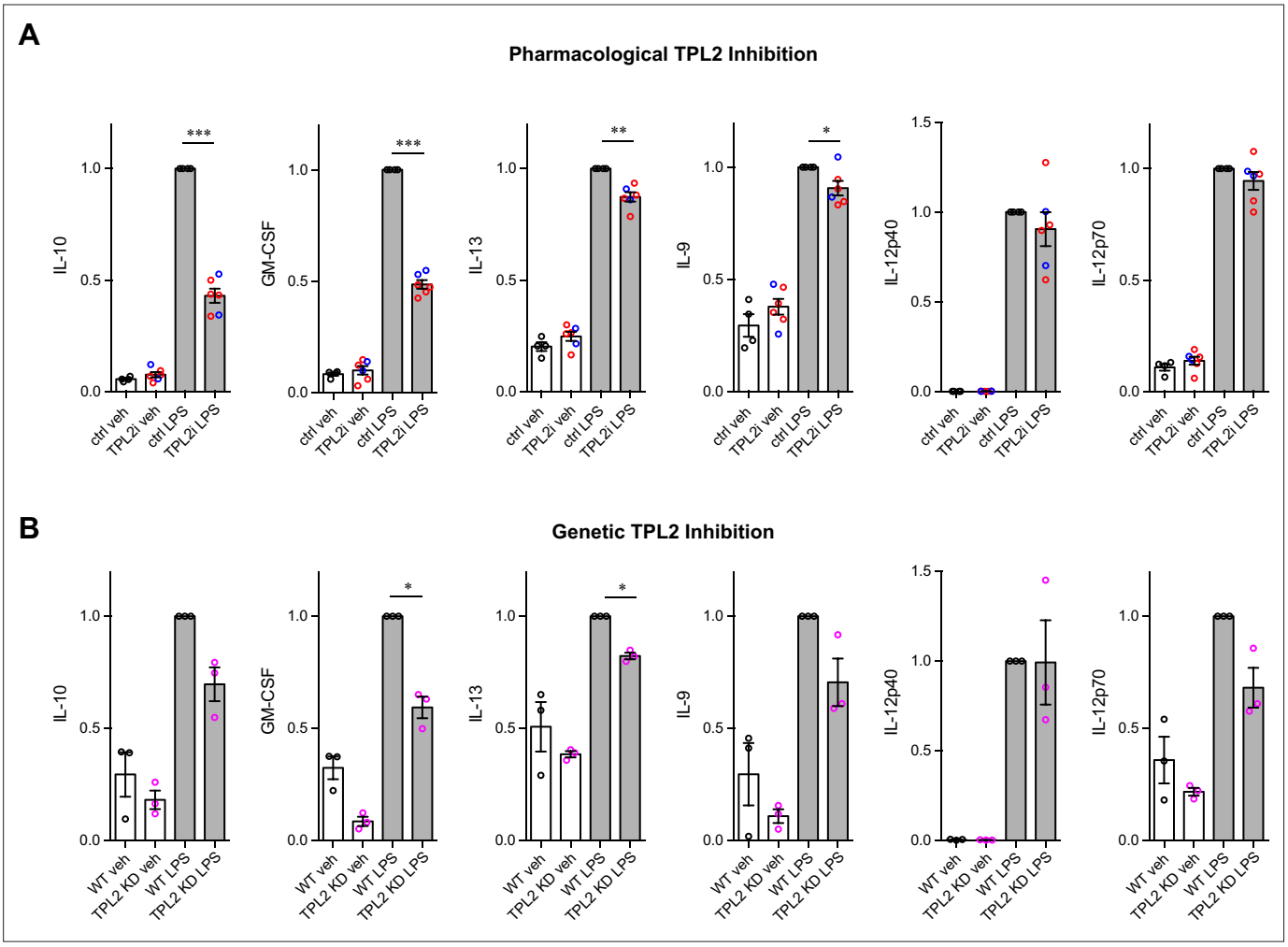

Figure 1—figure supplement 3. Cytokine and chemokine release by microglia after lipopolysaccharide (LPS) stimulation. Additional cytokine and chemokine measurements from the same samples as shown in ***Figure 1C and D*** are shown here. Cytokine and chemokine levels from the supernatants of WT primary microglia with or without TPL2 inhibitor (**A**) or microglia isolated from WT mice or tumor progression locus 2 kinase dead (TPL2-KD) mice (**B**) under control or LPS induction (24 hr incubation) conditions as indicated. Data are represented by mean ± SEM. *, p<0.05, **, p<0.01, ***, p<0.001, one-way ANOVA with Tukey's multiple comparisons test.

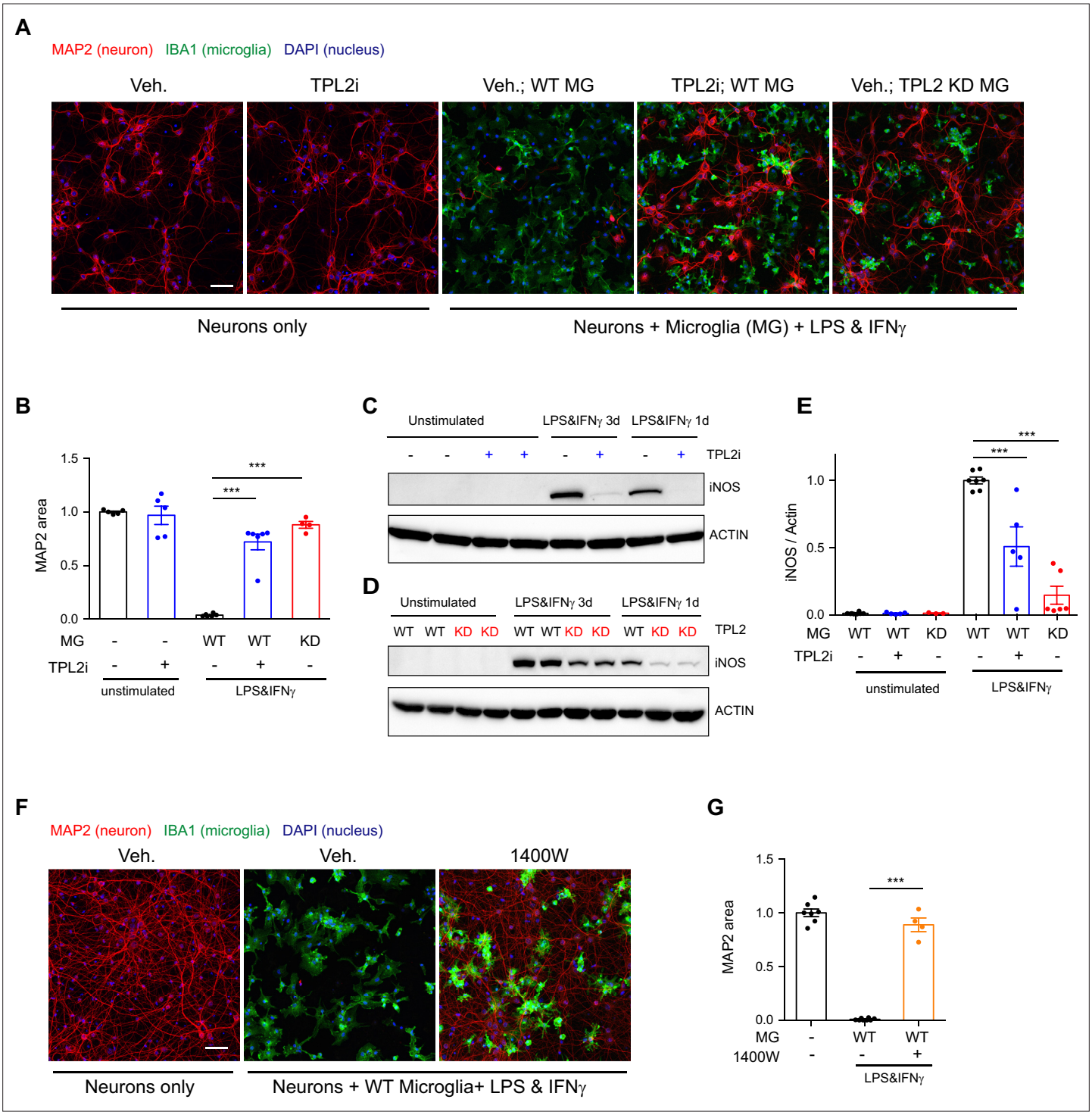

Figure 2. Tumor progression locus 2 (TPL2) inhibition rescues neurodegeneration in a co-culture model. (**A**) Representative images of immunostaining for MAP2 (red), IBA1 (green), and DAPI (blue) in mouse cortical neuronal cultures or mouse cortical neurons co-cultured with mouse microglia as indicated. Cell number ratio in co-cultures is 1:1. Neurons were always cultured from WT mice and microglia were either from WT mice or TPL2 kinase dead (TPL2-KD) mice as indicated. Scale bar, 50 µm. (**B**) Quantification of MAP2 staining positive area within the image field as a readout of surviving neurons in the culture. MAP2 area is shown as normalized relative to the average value of the control condition (no microglia, no stimulation). n=5–6 per condition. (**C** and **D**) Representative immunoblots of iNOS (inducible nitric oxide synthase) from primary microglia cultures with treatments as indicated. Comparison was done either between WT microglia treated with and without TPL2 inhibitor G-767 (**C**), or between microglia isolated from WT mice and TPL2-KD mice (**D**). (**E**) Quantification of western blot data in (**C**) and (**D**). iNOS signal was normalized to actin signal, and the normalized values were plotted relative to the average value of the lysates from WT microglia treated with lipopolysaccharide (LPS) and interferon gamma. n=3–8.

Figure 2 continued on next page

Figure 2 continued

(**F**) Representative images of immunostaining of MAP2 (red), IBA1 (green), and DAPI (blue) in mouse cortical neuronal cultures or mouse cortical neurons co-cultured with mouse microglia as indicated. Cell number ratio in co-cultures is 1:1. Scale bar, 50 μm. (**G**) Quantification of MAP2 staining is shown as in (**B**). n=4–8. For all bar graphs, data are represented by mean ± SEM. ***, p<0.001, one-way ANOVA with Tukey's multiple comparisons test.

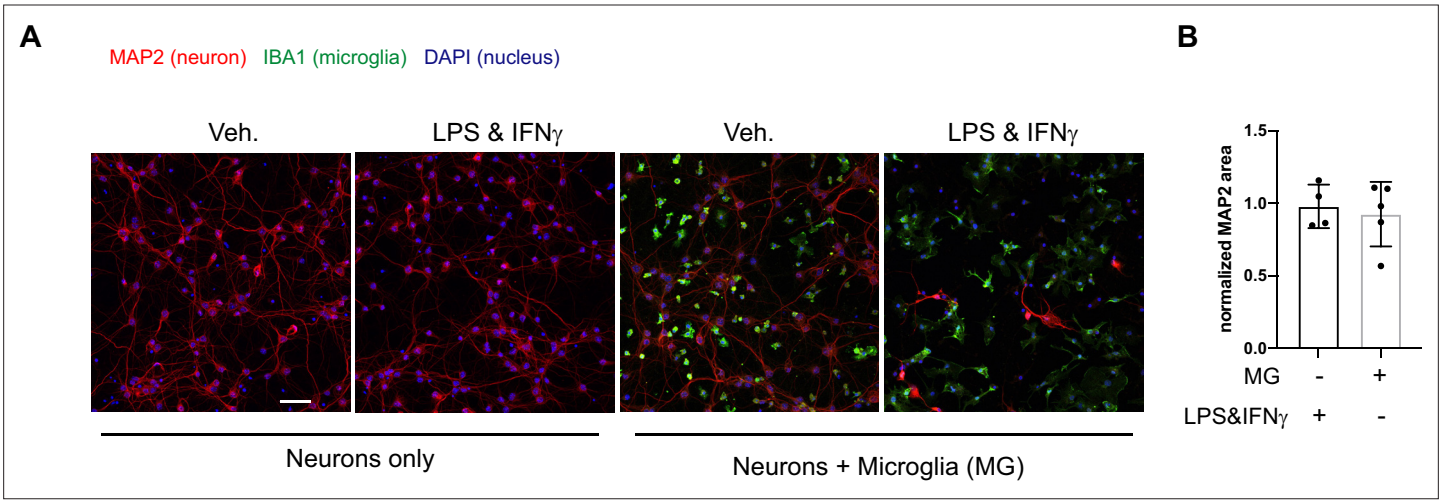

Figure 2—figure supplement 1. Stimulation of neurons cultured without microglia or co-culture of neurons and microglia without stimulation does not result in neuronal loss. (**A**) Representative images of immunostaining of MAP2 (red), IBA1 (green), and DAPI (blue) in mouse cortical neuronal cultures or mouse cortical neurons co-cultured with mouse microglia as indicated. Cell number ratio in co-cultures is 1:1. Neurons and microglia were both cultured from WT mice. Scale bar, 50 μm. (**B**) Quantification of MAP2 staining positive area within the image field as readouts of surviving neurons in the culture. MAP2 areas are shown as normalized relative to the average value of control condition (no microglia, no stimulation). n=4–5 per condition.

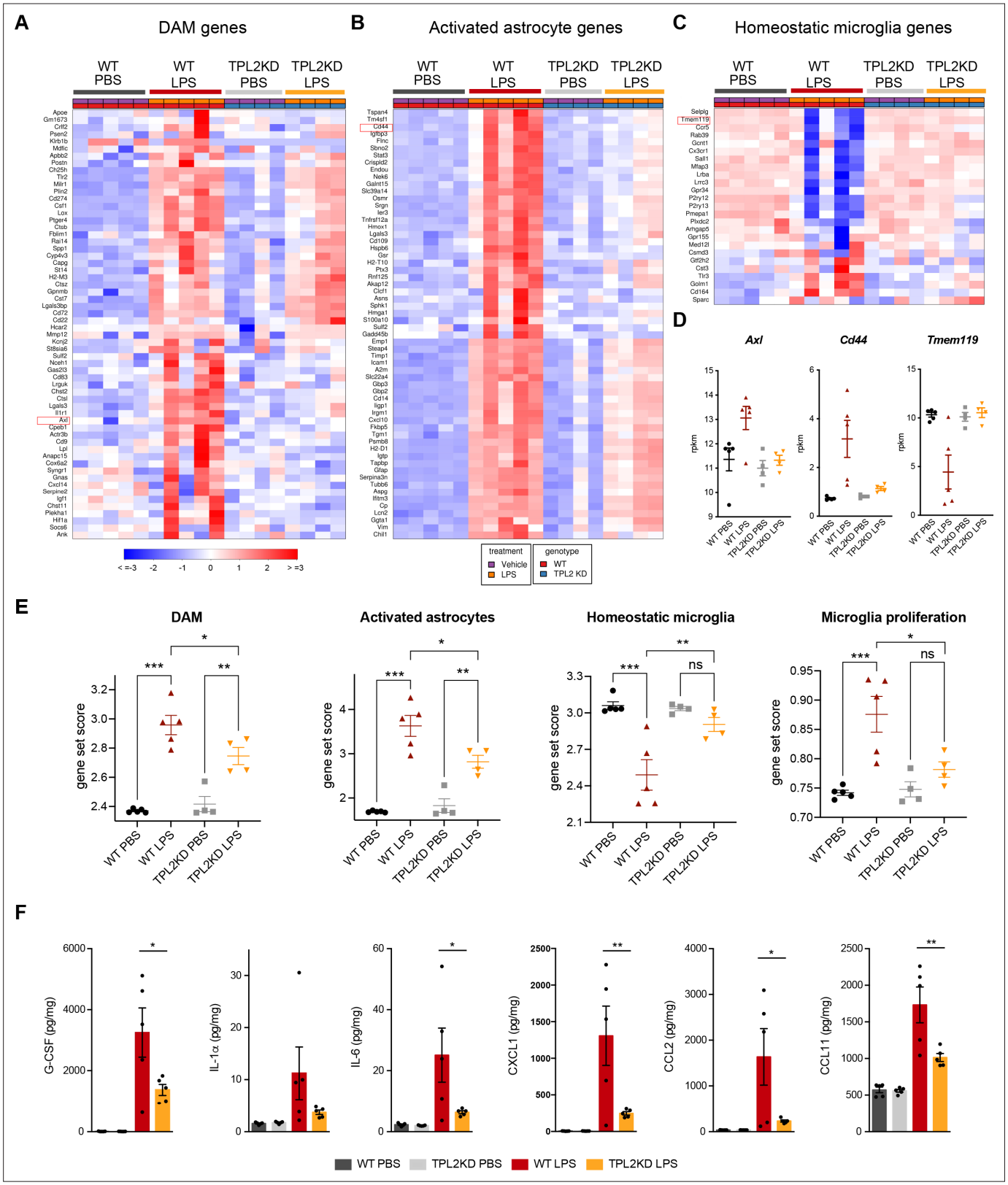

Figure 3. Tumor progression locus 2 kinase dead (TPL2-KD) mice have attenuated gene expression changes and cytokine/chemokine response after lipopolysaccharide (LPS) injection. (**A**) Heatmap showing z-scores of the top 60 DAM genes (disease-associated microglia genes) in the brains of WT or TPL2-KD mice harvested 24 hr post intraperitoneal injection with phosphate-buffered saline (PBS) or LPS (10 mg/kg). The top 60 DAM genes were taken from the list in ***Friedman et al., 2018***, and were selected based on the ranking of z-scores of these genes in WT mice injected with LPS. (**B**) Heatmap

Figure 3 continued on next page

Figure 3 continued

showing z-scores of the top 60 activated astrocyte genes taken from the list in ***Wu et al., 2019*** (both A1 and A2 astrocyte genes were included). The top 60 genes were also selected based on the ranking of z-scores of these genes in WT mice injected with LPS. (**C**) Heatmap showing z-scores of homeostatic microglia genes from ***Friedman et al., 2018***. (**D**) Examples of DAM genes (*Axl*), astrocyte-activated genes (*Cd44*), and homeostatic microglia genes (*Tmem119*). (**E**) Geneset score expression of DAM genes, activated astrocyte genes, homeostatic microglia genes, and microglia proliferation genes in mouse brain samples with different treatments as indicated. n=4–5 animals per condition. (**F**) Cytokine and chemokine levels in mouse brain lysates from the same mice as in (**A–E**) measured using a bead-based multiplex assay. Cytokine levels were normalized to total protein concentration in brain lysates and are shown as pg/mg. Only analytes that were above the detection level, changed after LPS injection, and exhibited a difference between WT and TPL2-KD mice are shown. Data are represented by mean ± SEM. *, $p<0.05$, **, $p<0.01$, ***, $p<0.001$, one-way ANOVA with Tukey's multiple comparisons test.

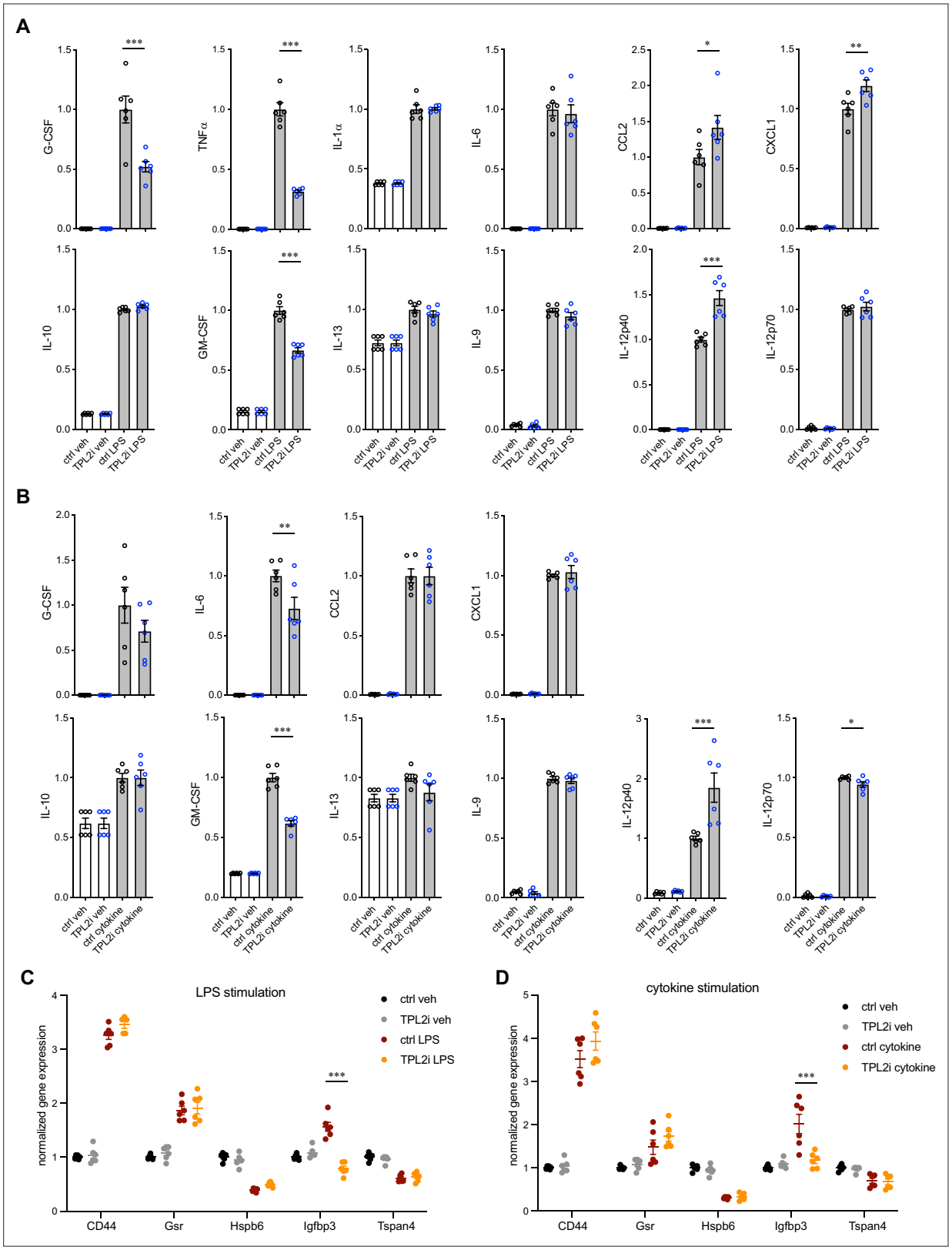

Figure 3—figure supplement 1. Cell-autonomous role of tumor progression locus 2 (TPL2) in activated astrocytes. (**A and B**) Quantification of cytokine measurements from the supernatants of primary astrocyte cultures stimulated with lipopolysaccharide (LPS) (**A**) or TNFα+IL-1α (**B**) with or without TPL2 inhibitor G-767 (24 hr incubation). Cytokines shown here are the same as shown for the primary microglia study (***Figure 1*** and Figure 1-figure supplement 3). Cytokine measurements were normalized to average values of stimulated astrocytes without inhibitor. n=6 from two independent

Figure 3—figure supplement 1 continued on next page

Figure 3—figure supplement 1 continued

cultures. (**C and D**) RT-qPCR analysis of RNA extracted from primary astrocyte cell lysates under the same conditions as in (**A**) and (**B**). Gene expression was first normalized to GAPDH and then normalized to expression under control condition. Data are represented by mean ± SEM. *, p<0.05, **, p<0.01, ***, p<0.001, one-way ANOVA with Tukey's multiple comparisons test.

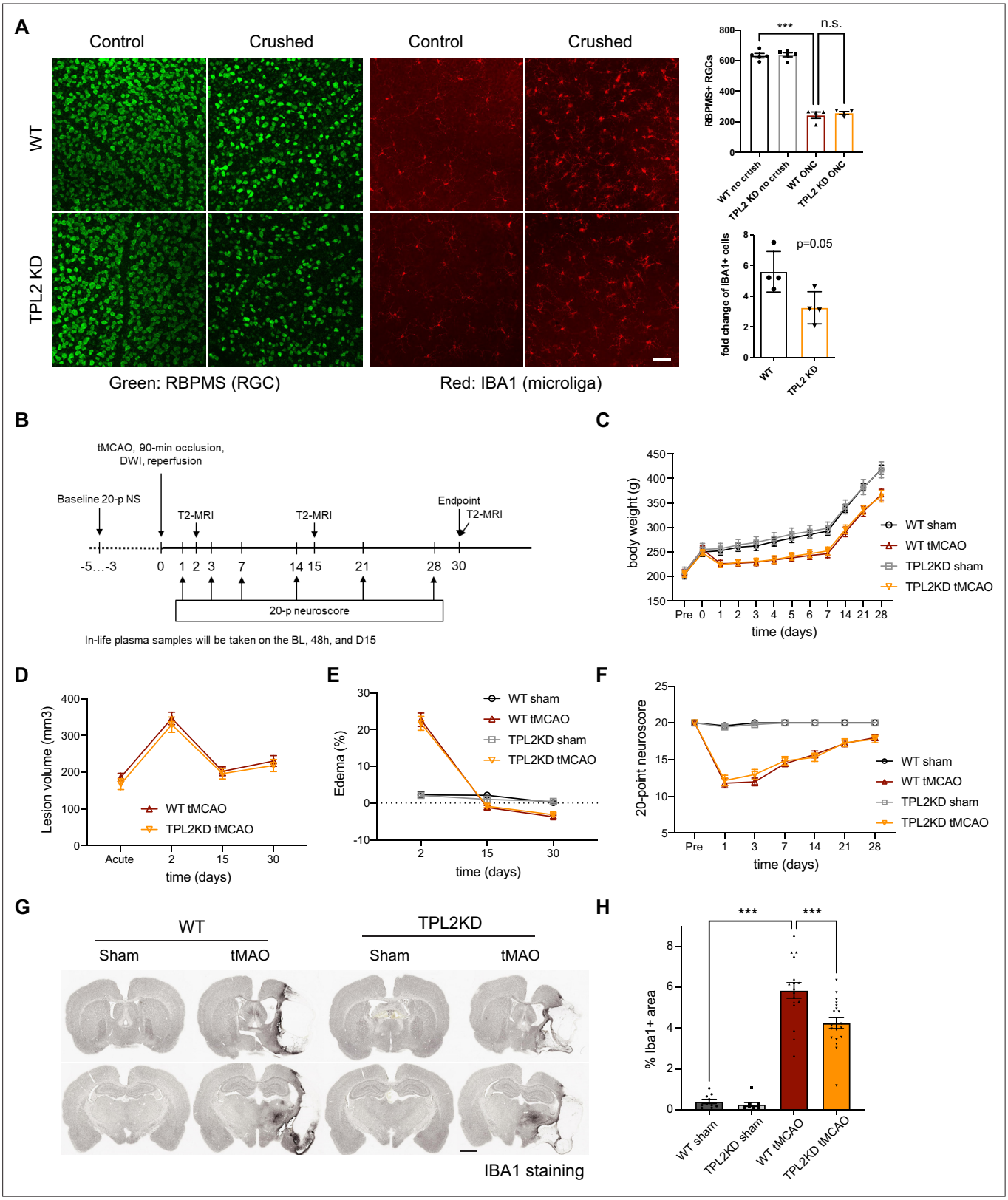

Figure 3—figure supplement 2. Effect of tumor progression locus 2 kinase dead (TPL2-KD) in acute injury models: optic nerve crush (ONC) and stroke. (**A**) *Left*, representative images of whole-mount retina stained with RBPMS (green) for retinal ganglion cells (RGCs) and IBA1 (red) for microglia/macrophages from control eye or ONC eye of WT or TPL2-KD mice as indicated. Scale bar, 50 μm. *Top right*, quantification of the cell number of RGCs. *Bottom right*, quantification of the ratio of Iba1 positive cell number in the ONC eye relative to the control eye of the same mouse. Each dot represents

Figure 3—figure supplement 2 continued on next page

Figure 3—figure supplement 2 continued

one mouse. Data are represented by mean ± SEM. ***, p<0.001, one-way ANOVA with Tukey's multiple comparisons test. (**B**) Experimental design of rat tMAO study. (**C**) Bodyweight measurements of WT and TPL2-KD rats after sham or tMAO surgery at multiple timepoints as indicated. (**D**) Quantification of lesion volume based on volumetric analysis of T2 relaxation time analysis from T2-MRI of WT or TPL2-KD rats after tMAO surgery. (**E**) Quantification of percentage of tissue area with edema from T2-MRI of WT or TPL2-KD rats after sham or tMAO surgery. (**F**) Behavioral analysis of WT or TPL2-KD rats after sham or tMAO surgery as indicated using 20-point neuroscore measurement. (**G**) Representative images of Iba1 staining in WT and TPL2-KD rats 30 days post sham or post tMAO as indicated. Scale bar, 2 mm. (**H**) Quantification of percentage of tissue area that are positive for Iba1 staining in the ipsilateral side of the rat brains. One mouse brain was excluded as outlier based on Grubb's test. Data are represented by mean ± SEM. n=10 for WT sham, n=17 for WT tMAO, n=9 for TPL2-KD sham, n=19 for TPL2-KD tMAO. ***, p<0.001, one-way ANOVA with Tukey's multiple comparisons test.

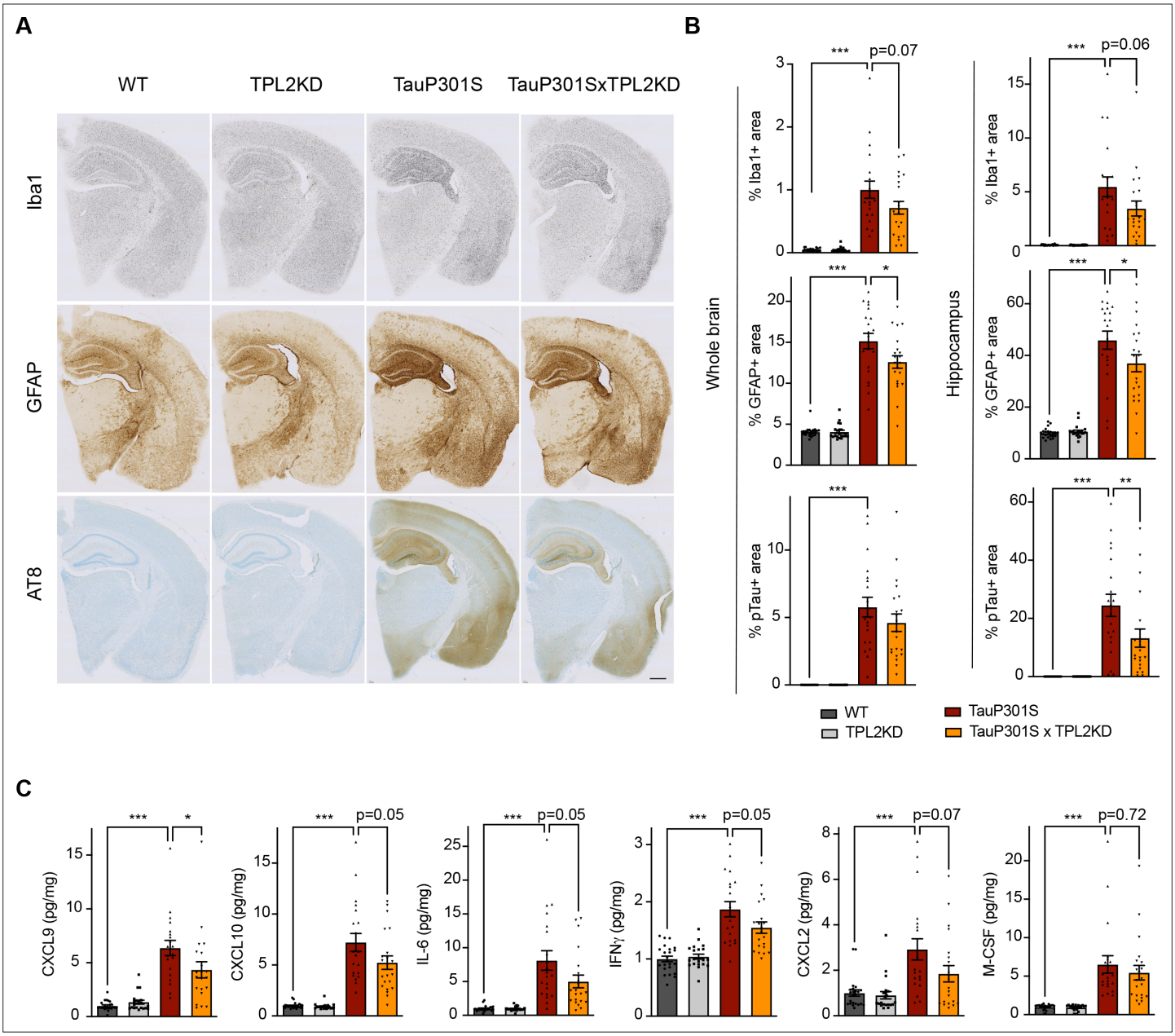

Figure 4. Tumor progression locus 2 kinase dead (TPL2-KD) partially rescues neuroinflammation in TauP301S mouse brain. (**A**) Representative images showing immunostaining for Iba1, GFAP, and AT8 in mouse hemi-brains from 9-month-old male mice with genotypes as indicated. Scale bar, 500 μm. (**B**) Quantification of percentage of Iba1, GFAP, AT8 positive area within mouse hemi-brains and specifically within the hippocampus as indicated. Analysis shown are combined data from 9-month-old male mice and 11-month-old female mice. Each dot represents one animal. (**C**) A subset of cytokines or chemokine levels in mouse hippocampal lysates measured using bead-based mouse cytokine multiplex assay. Cytokine levels were normalized to total protein concentration in brain lysates and are shown as pg/mg. Data shown include protein levels from both 9-month-old male mice and 11-month-old female mice. For all bar graphs, data are represented by mean ± SEM. *, p<0.05, ***, p<0.001, one-way ANOVA with Tukey's multiple comparisons test.

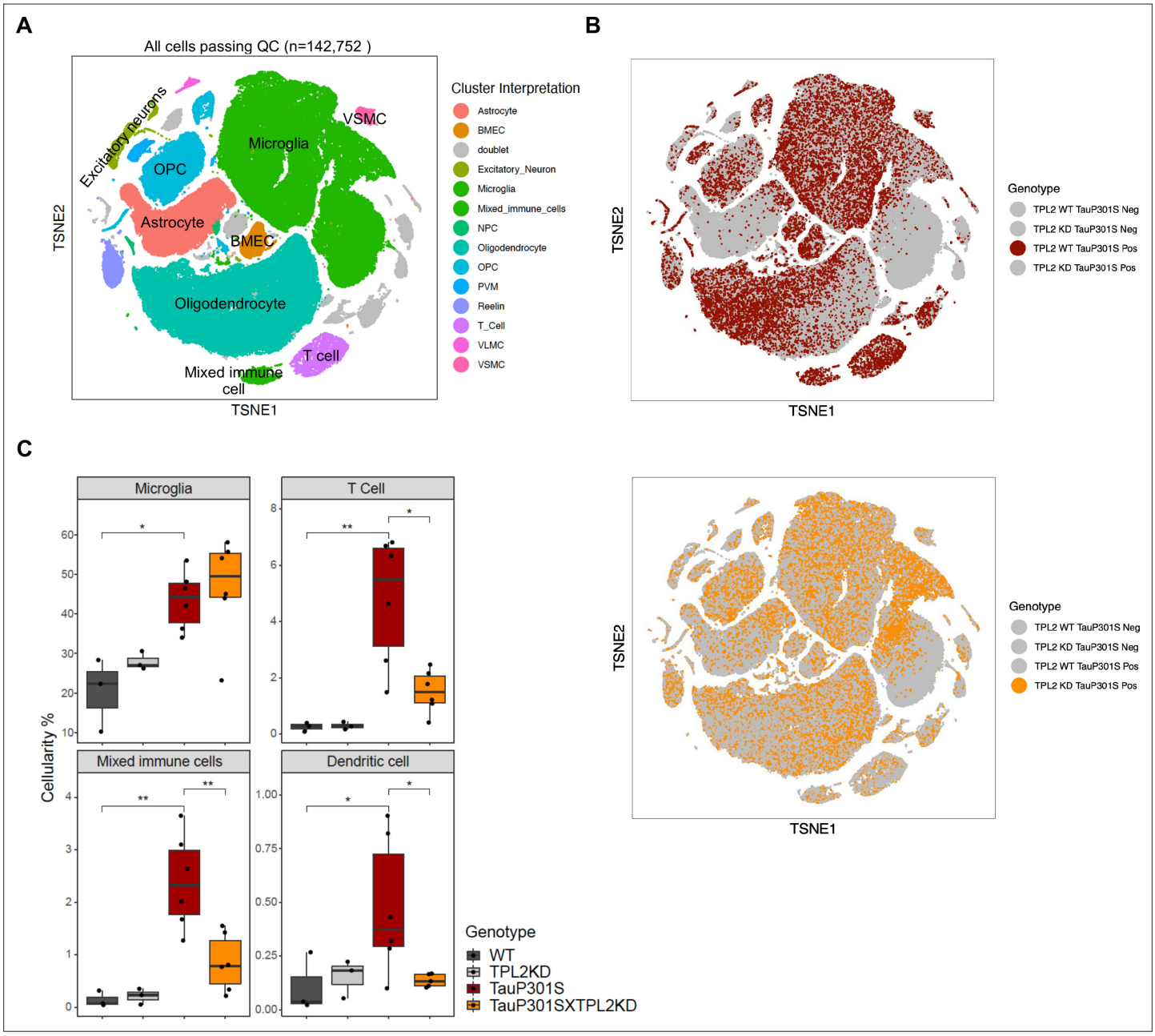

Figure 5. Single-cell RNA sequencing (scRNA-seq) shows that tumor progression locus 2 kinase dead (TPL2-KD) normalizes increased T-cells and dendritic cells in TauP301S brains. (**A**) tSNE dimensional reduction and cell type interpretation of 142,752 hippocampal cells from 9-month-old TPL2 WT/KD TauP301S positive/negative mice. (**B**) Distribution of cells by TPL2 genotype in TauP301S positive samples. (**C**) 'Cellularity plot' illustrating proportions of microglia, mixed immune cells, T-cells, and dendritic cells as identified from further analysis of the mixed immune cell cluster described in ***Figure 5—figure supplement 3*** in each genotype. Each point represents a single animal, and the *y*-axis is the percentage of all cells in the scRNA-seq dataset for that animal of the given cell type. Boxplots showing summarized distribution of the percentage; p-values are based on t-test between indicated groups using ggpubr. *, p<0.05, **, p<0.01.

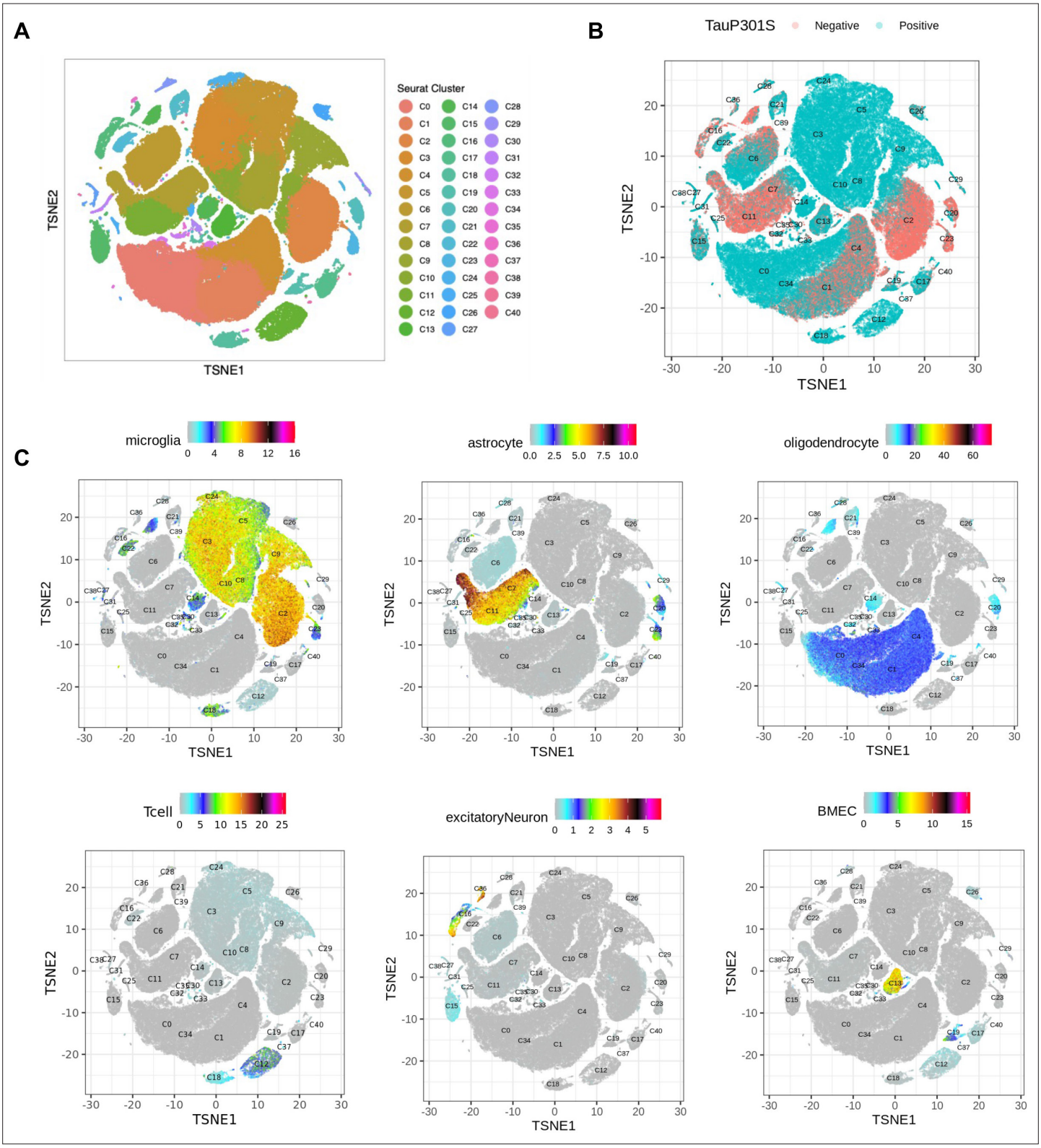

Figure 5—figure supplement 1. Dimensional reduction and interpretation of cell clusters by gene set scores. (**A**) tSNE dimensional reduction and cell type interpretation of 142,752 hippocampal cells from 9-month-old tumor progression locus 2 (TPL2) WT/kinase dead (KD) TauP301S positive/negative mice. (**B**) Distribution of cells by TauP301S phenotype. (**C**) tSNE plots of gene sets marking specific cell type populations based on cell type-specific markers from ***Lee et al., 2021b***. Gene sets can be found in ***Supplementary file 1***.

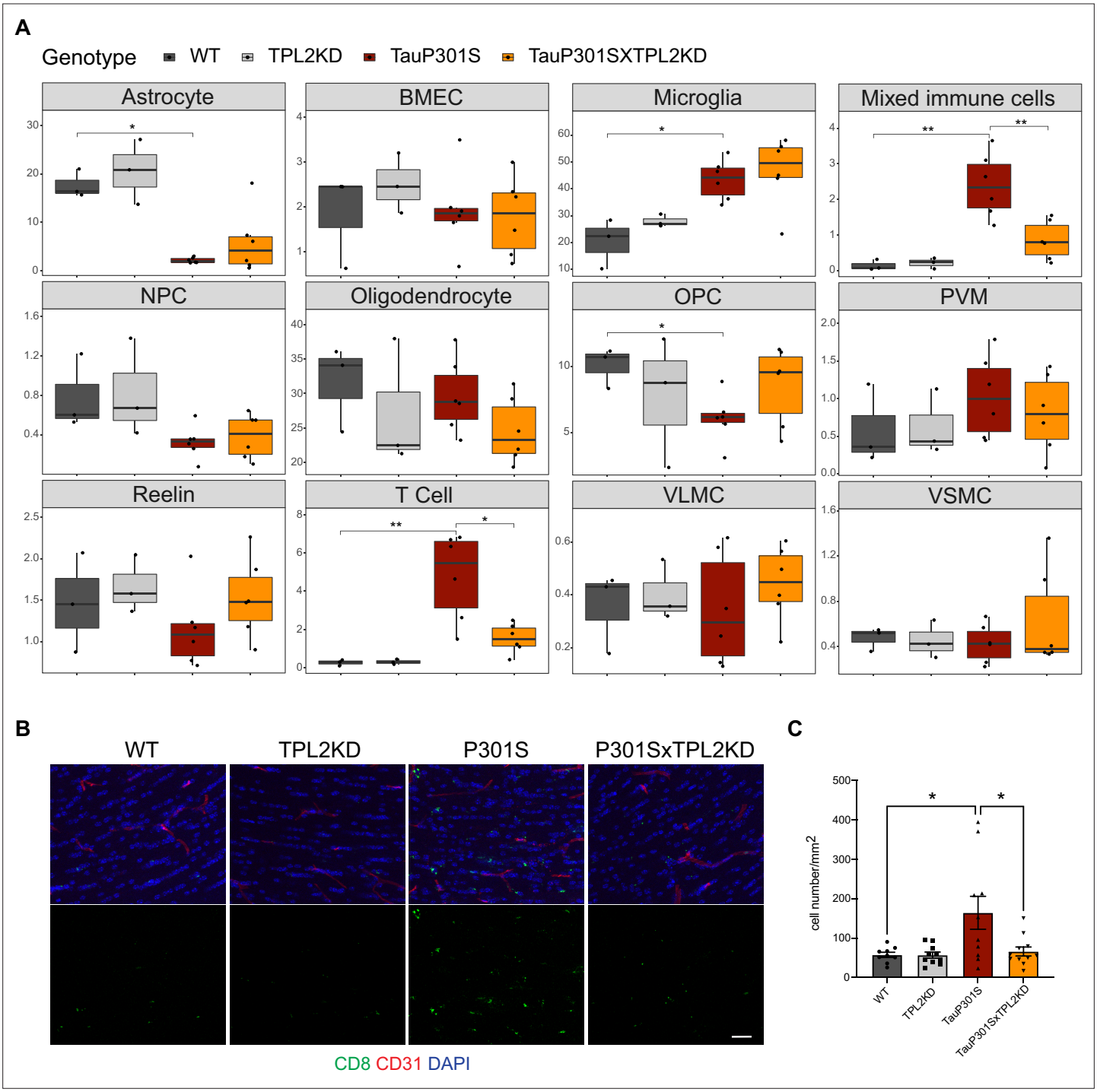

Figure 5—figure supplement 2. Cellularity plot for all initially annotated cell types and T-cell immunostaining. (**A**) Cellularity plots for each cell type from ***Figure 5A***. The percentage of cells in each cell type is plotted as a percentage of the total number of cells within each sample (each dot is a sample). p-Values are based on t-test between indicated groups. *, p<0.05, **, p<0.01. (**B**) Representative images of fimbria immunostaining of brain sections from mice with indicated genotypes using CD8 (green) to stain T-cells and CD31 (red) for vasculature. Scale bar, 25 μm. (**C**) Quantification of CD8 positive T-cells in fimbria by immunostaining. Data are represented by mean ± SEM. n=9–11 animals per genotype. *, p<0.05, one-way ANOVA with Tukey's multiple comparisons test.

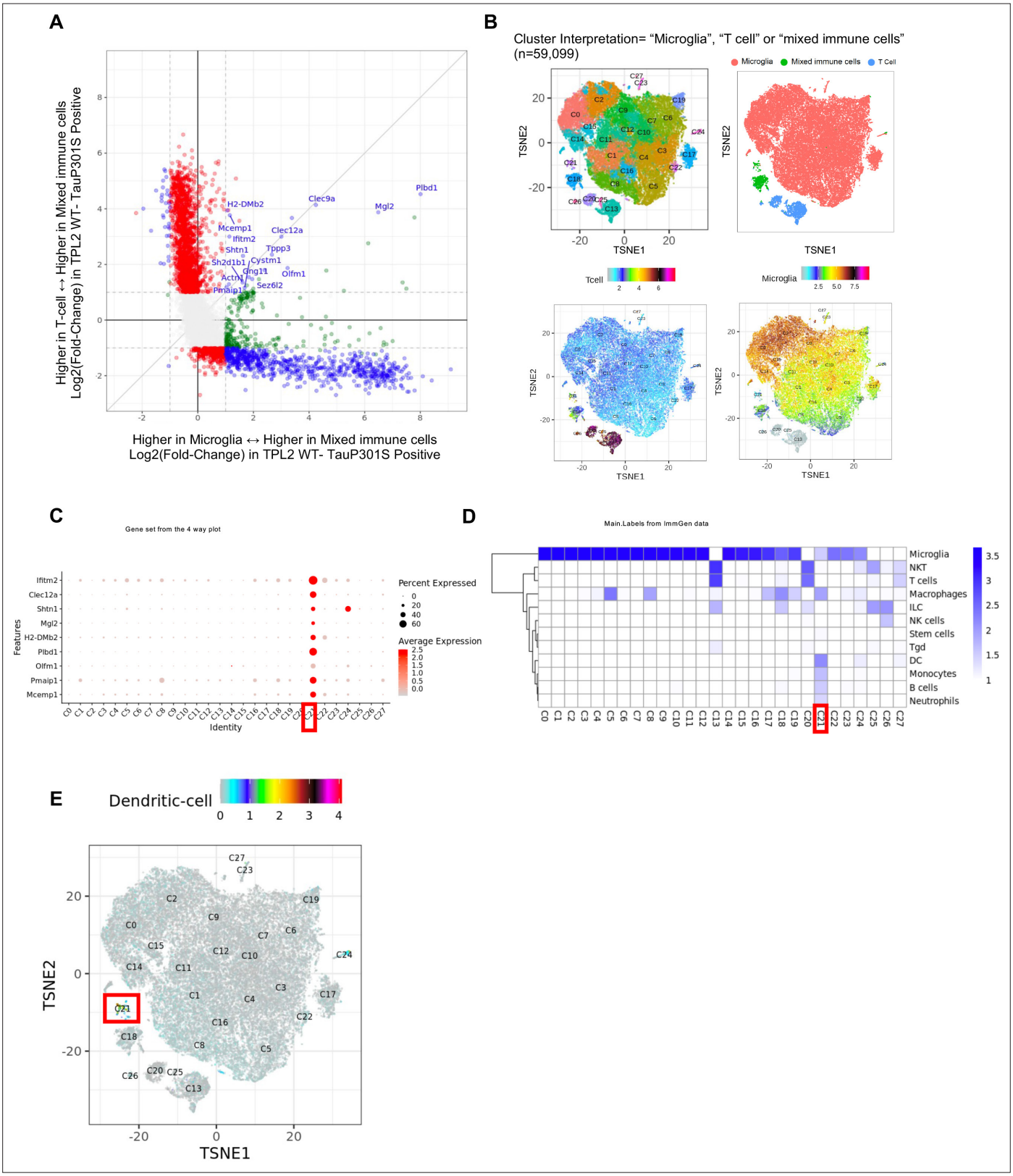

Figure 5—figure supplement 3. Identification of a unique cluster within the 'mixed immune cell' cluster that corresponds to dendritic cells. (**A**) Scatter plot comparing gene expression fold-changes from T-cell vs. mixed immune cell cluster (*x*-axis) against fold-changes from microglia vs. mixed immune cell clusters, as identified in ***Figure 5A***. Genes called as significantly differentially expressed (FDR <0.05, log2(fold-change) >1 or < –1) are colored in red (T-cell vs. mixed immune cell), green (microglia vs. mixed immune cell), or blue (both contrasts). *x* and *y* axes represent gene expression on a log2

Figure 5—figure supplement 3 continued on next page

Figure 5—figure supplement 3 continued

scale (log2(normCount + 1)). Genes significantly enriched in mixed immune cell versus both microglia and T-cell populations are labeled, and these are potential candidate markers for a unique subpopulation of the mixed immune cell that are distinct from microglia and T-cells. (**B**) tSNE dimensional reduction of immune cells (n=59,099; microglia n=54,523, T-cell n=2977 and mixed immune cells n=1599), colored by subcluster, major cluster from ***Figure 5A***, or T-cell (***Lee et al., 2021b***) or resting microglia (***Friedman et al., 2018***) gene set scores (gene sets in ***Supplementary file 1***). Of note, C18 are microglia and T-cell doublets. (**C**) Dot plot showing the expression of potential candidate markers for the unique mixed immune subpopulation (as labeled in (**A**)) that are also identified as potential markers for immune cell subcluster C21 using FindMarkers function from Seurat package (***Stuart et al., 2019***). (**D**) Heatmap showing prediction scores for immune cell subclusters using SingleR and ImmGen dataset main labels (***Heng and Painter, 2008***) from the celldex package (***Aran et al., 2019***). This analysis indicates that the unique cell population in C21 most strongly corresponds to dendritic cells (DC). (**E**) tSNE plot of genes marking C21 (dendritic) population using potential markers from (**A**).

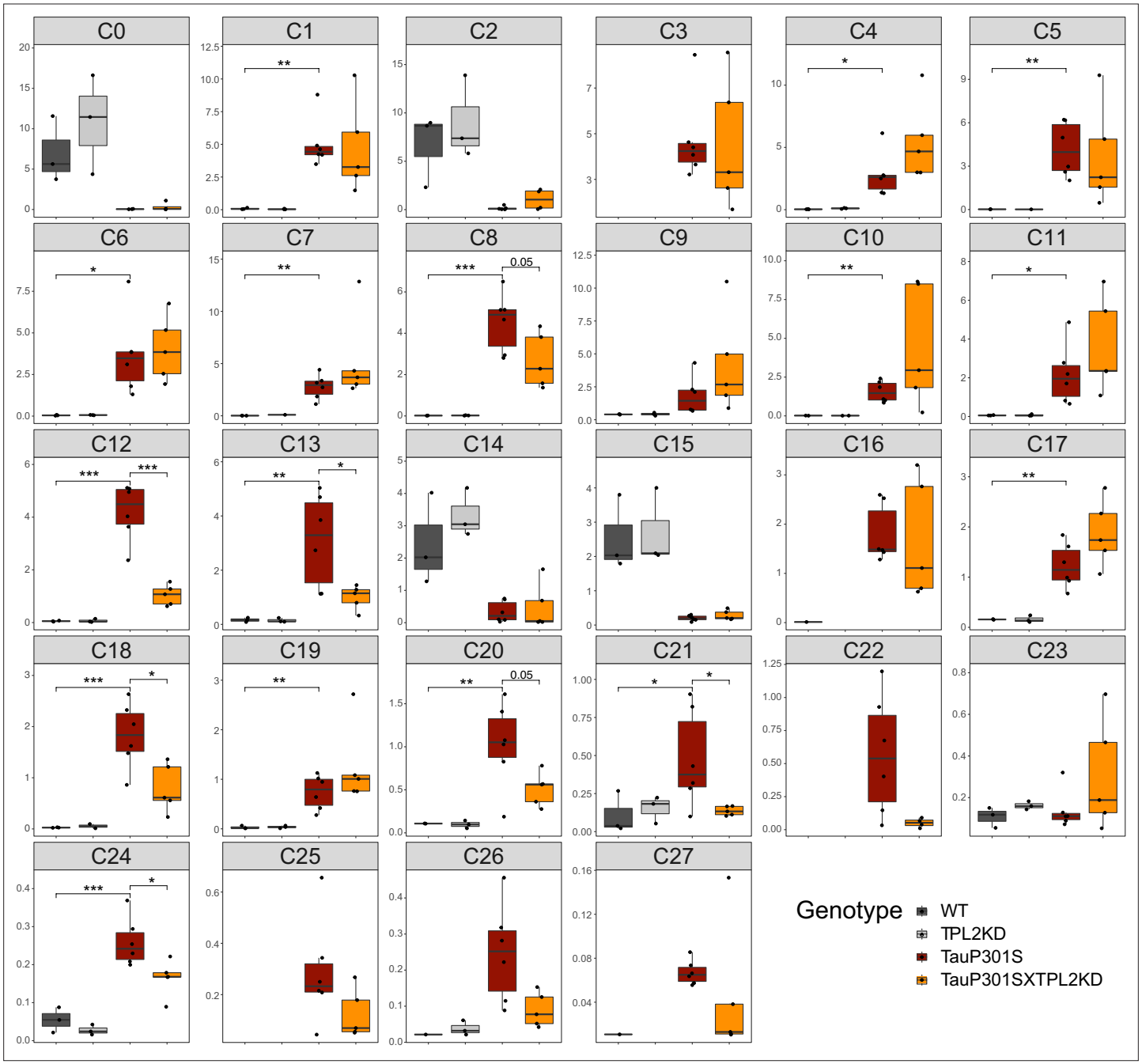

Figure 5—figure supplement 4. Cellularity plot for all immune cell subclusters. Proportions of immune cell subclusters (from ***Figure 5—figure supplement 3B***) as a percentage of total immune cells within each sample (each dot is a sample). p-Values are based on t-test between indicated groups. *, p<0.05, **, p<0.01, ***, p<0.001.

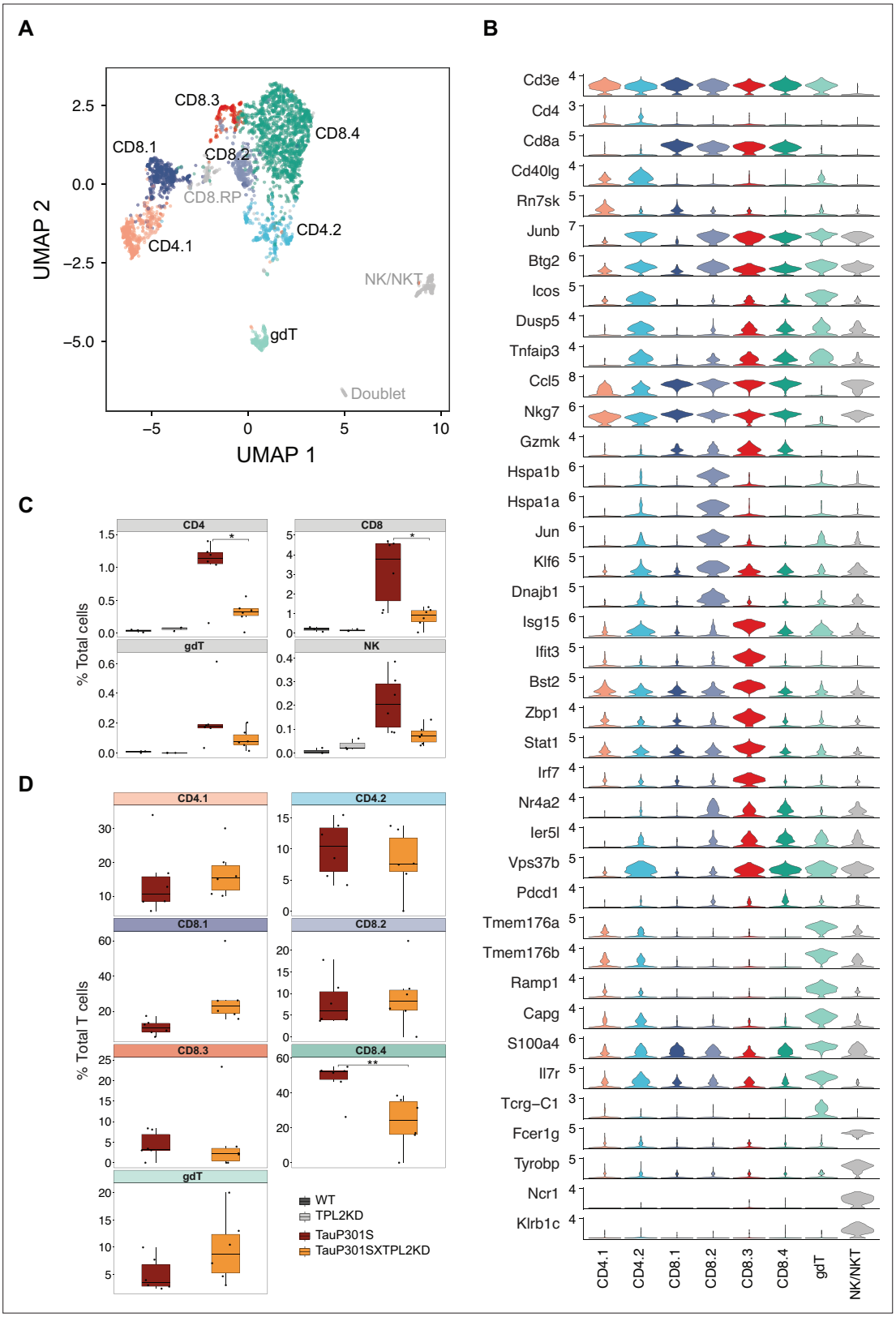

Figure 5—figure supplement 5. Subclustering of T-cells. (**A**) UMAP dimensionality reduction and subclustering of 2977 T-cells defined from ***Figure 5A***, colored by cell type interpretation. gdT = Gammadelta T-cell, NK = natural killer, RP = ribosomal protein. (**B**) Violin plots showing the log2 normalized expression of select genes representative for cell types identified in (**A**). (**C–D**) Cellularity plot, similar to ***Figure 5C***, showing for each sample the percentage of T-cell subtypes as a percentage of the total number of cells (**C**) or the total number of T-cells (**D**) in that sample. p-Values are based on pairwise t-test with *Benjamini-Hochberg* correction for multiple comparisons in (C) or t-test in (**D**). *, p<0.05, **, p<0.01.

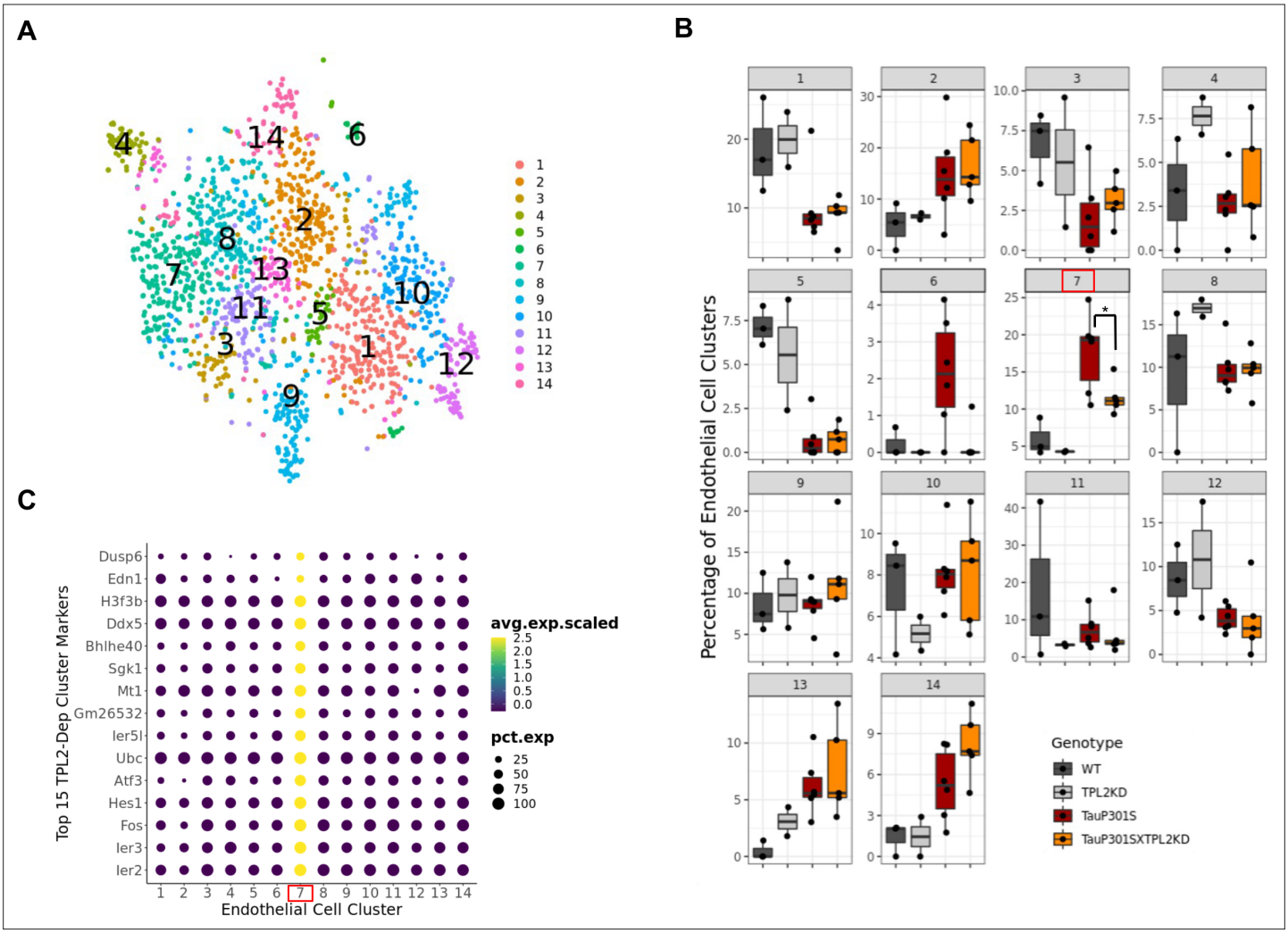

Figure 5—figure supplement 6. Subclustering of endothelial cells identifies a tumor progression locus 2 (TPL2)-dependent subcluster induced by TauP301S. (**A**) tSNE dimensional reduction of the endothelial cell subset from ***Figure 5A***, labeled by cluster number. (**B**) Percentage of endothelial cells in each cluster as a percentage of the total number of endothelial cells is shown for each genotype (each dot is a sample). p-Values are based on t-test between indicated groups using ggpubr. *, p<0.05. (**C**) Top 15 markers returned by Seurat's FindAllMarkers function for the TPL2-dependent subcluster 7.

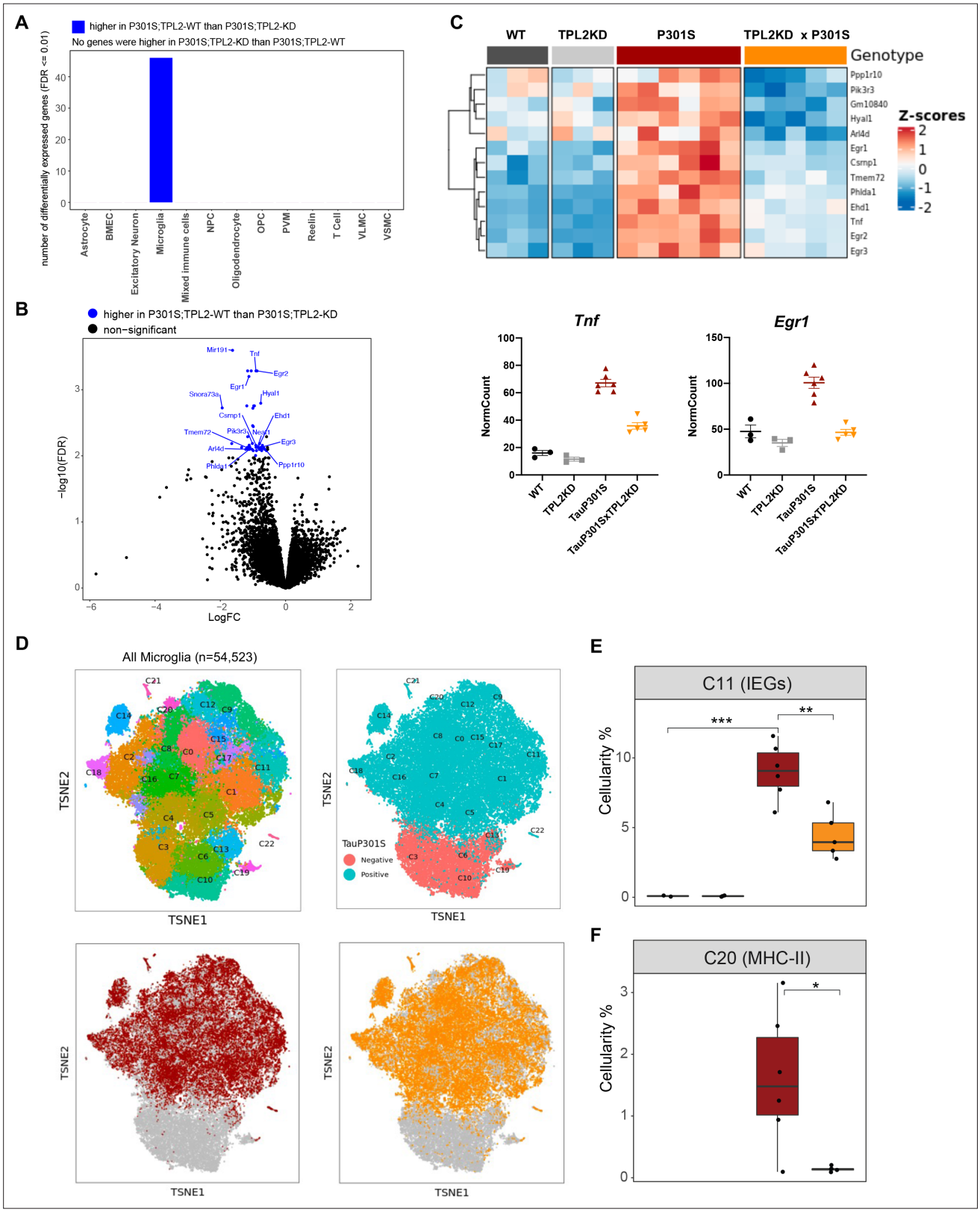

Figure 6. Tumor progression locus 2 kinase dead (TPL2-KD) partially normalizes elevated gene expression in TauP301S microglia and reduces the abundance of microglia in specific P301S-induced clusters. (**A**) Number of significantly differentially expressed genes (DEGs) for each cell type from pseudo-bulk analysis at FDR < 0.01 and log2(fold-change) >1.5 or <–1.5 between P301S and P301S;TPL2-KD genotypes. (**B**) Volcano plot showing DEGs for microglia from pseudo-bulk analysis between P301S and P301S;TPL2-KD genotypes. Only protein-coding genes were annotated. (**C**) Heatmap

Figure 6 continued on next page

Figure 6 continued

showing z-scores of log2(normCount + 1) for microglia DEGs as shown in (**B**). Boxplots summarizing expression levels of selected genes from the heatmap using normalized counts across the four genotypes used in this study. (**D**) tSNE-based subclustering of n=54,523 microglia defined from ***Figure 5A***, colored by subcluster identity and genotypes. (**E** and **F**) Cellularity plot, similar to ***Figure 5C***, showing for each sample the percentage of microglia in subclusters C11 or C20 as a percentage of the total number of microglia cells in that sample. p-Values are based on t-test between indicated groups. *, $p<0.05$, **, $p<0.01$.

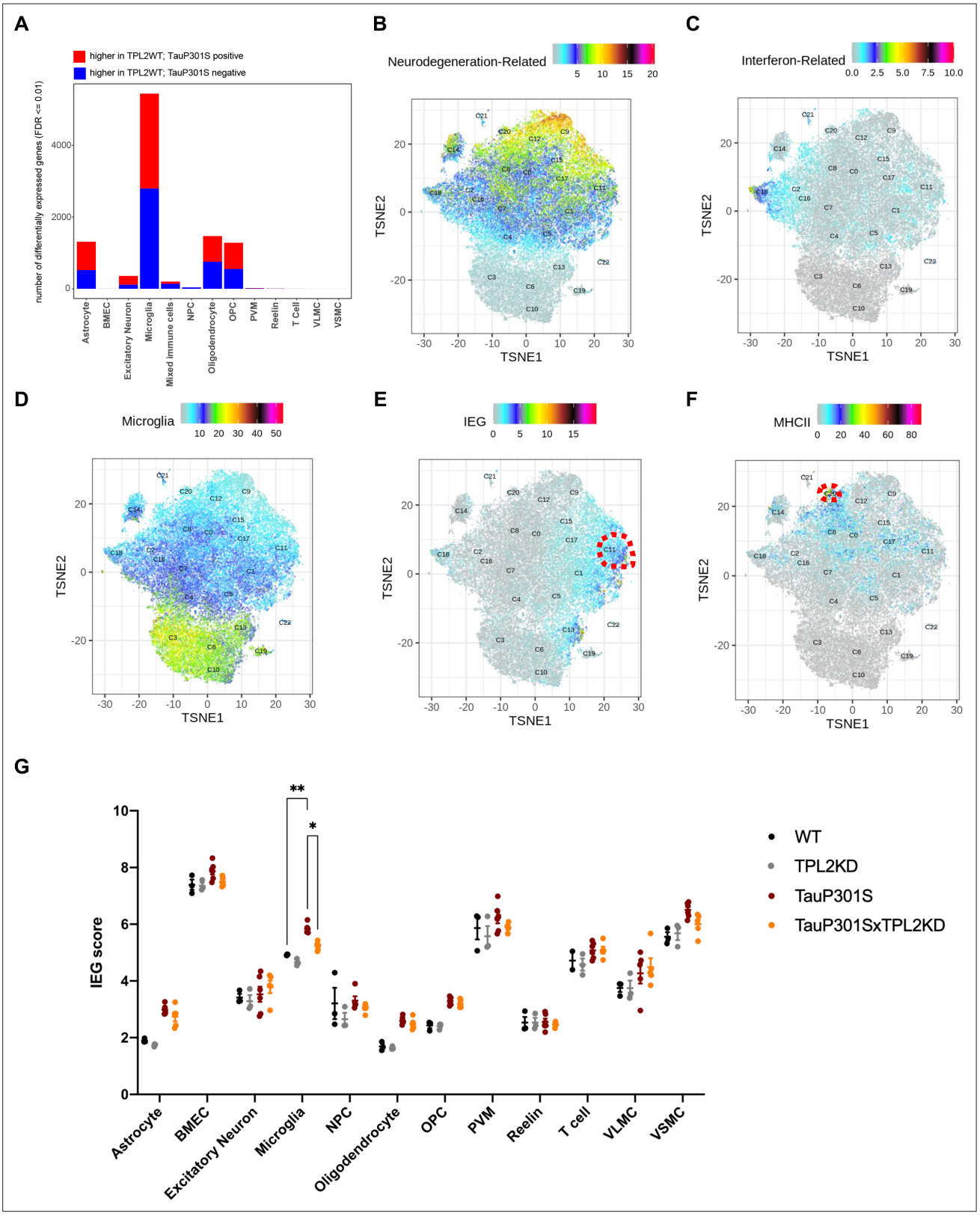

Figure 6—figure supplement 1. Subclustering of microglia and interpretation of cell activation states by gene set scores. (**A**) Number of significantly differentially expressed genes (DEGs) for each cell type from pseudo-bulk analysis at FDR <0.01 and log2(fold-change) >1.5 or <–1.5 between TauP301S positive and non-transgenic samples (TauP301S negative) across cell types from ***Figure 5A***. (**B–F**) tSNE dimensional reduction of microglia cells (n=54,523) colored by average/combinatorial expression of genes belonging to the indicated sets (disease-associated microglia [DAM], IFN, resting

Figure 6—figure supplement 1 continued on next page

Figure 6—figure supplement 1 continued

MG, immediate early gene [IEG], and MHCII). All gene sets used in this study are provided in ***Supplementary file 1***. (**G**) Strip plot showing expression levels of IEG gene sets in each of the four genotypes in this study across all cell types from ***Figure 5A***. Data are represented by mean ± SEM. *, p<0.05, **, p<0.01, ***, p<0.001, two-way ANOVA with Tukey's multiple comparisons test.

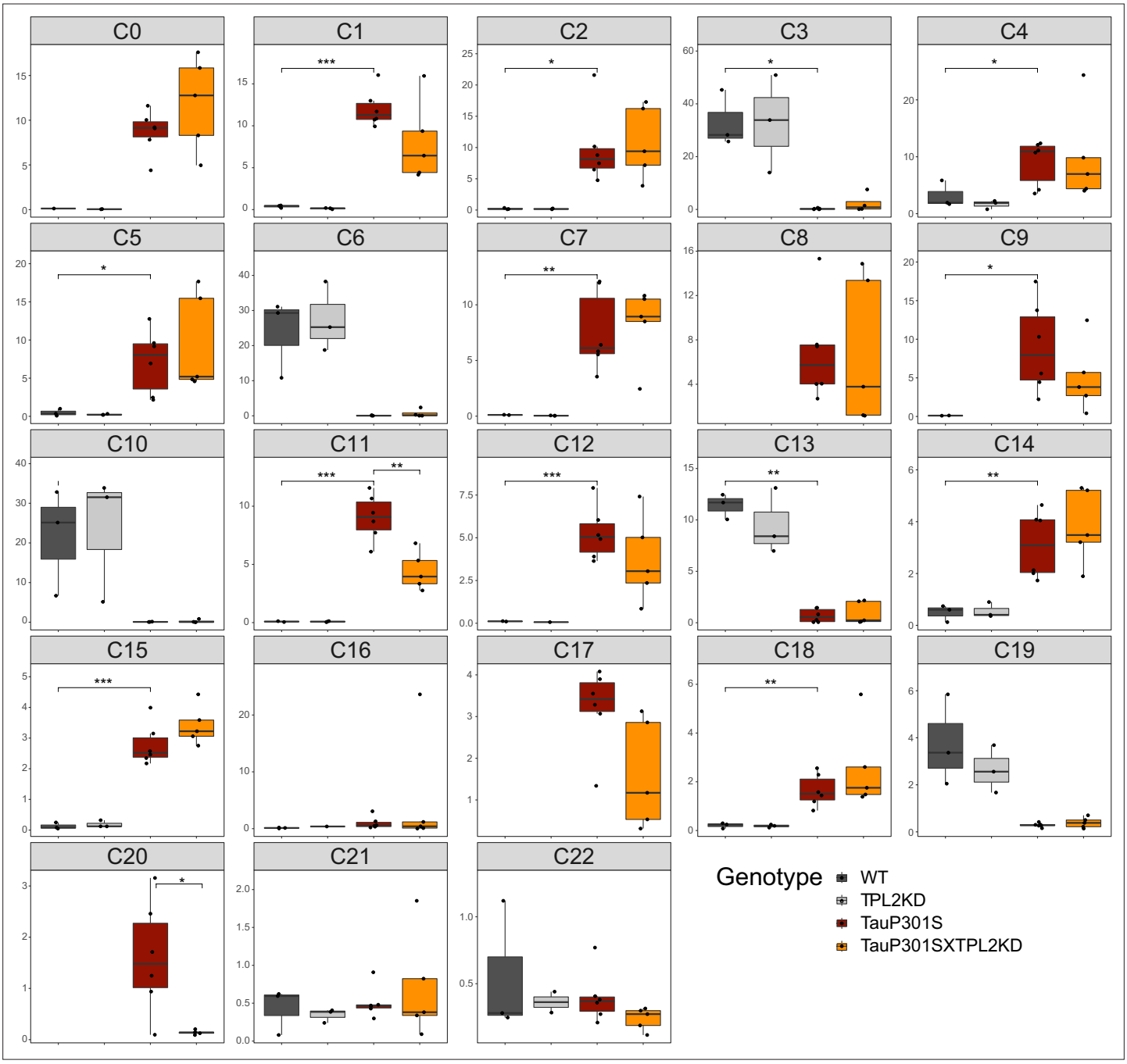

Figure 6—figure supplement 2. Cellularity plot for microglia cells. Similar to ***Figure 5C***, illustrating proportions of each microglia subcluster as a percentage of total microglia cells within each sample (each dot is a sample). p-Values are based on t-test between indicated groups. *, p<0.05, **, p<0.01, ***, p<0.001.

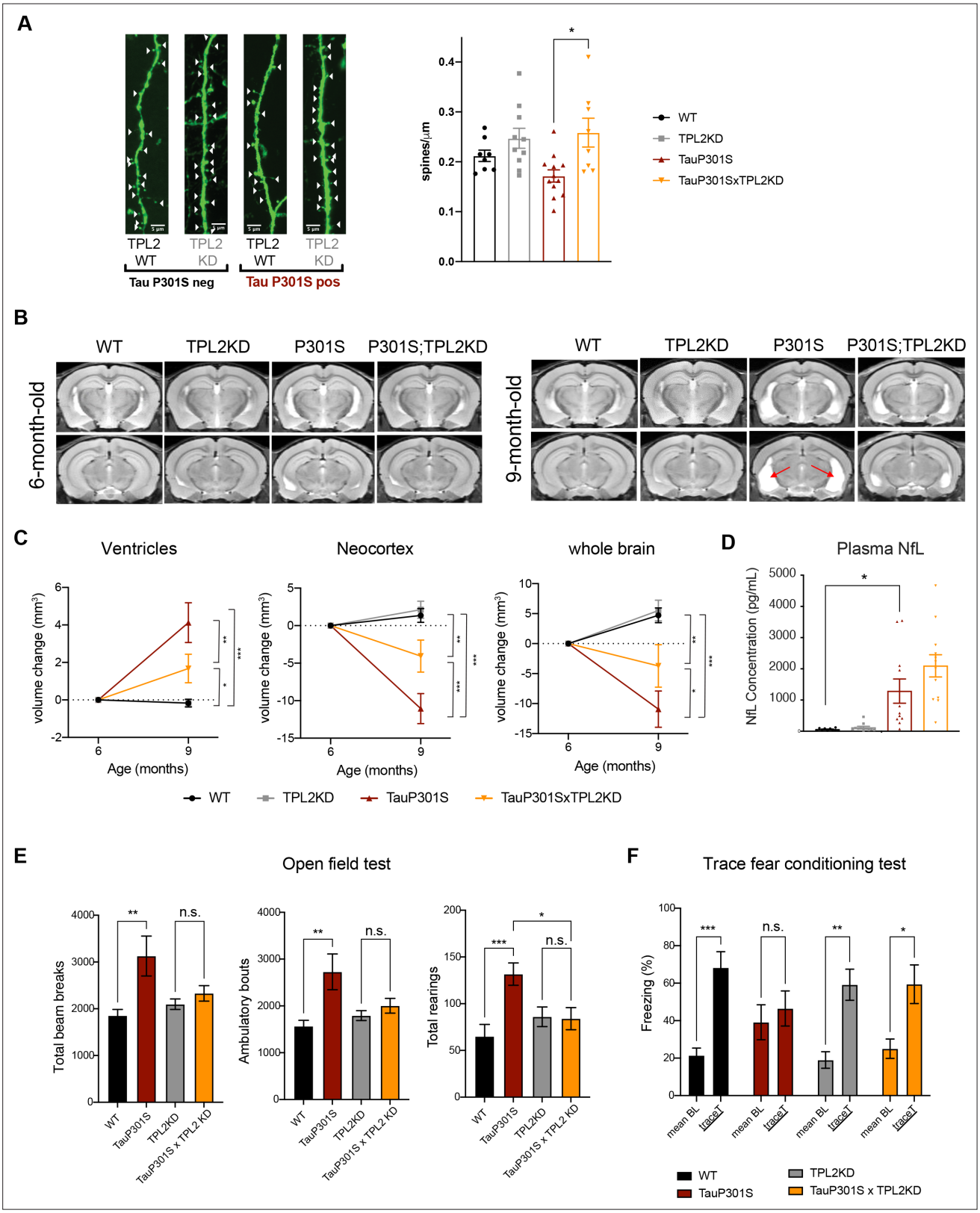

Figure 7. Tumor progression locus 2 (TPL2) functional deficiency attenuates brain atrophy and rescues behavioral deficits in TauP301S mice. (A) Ex vivo imaging of fixed mouse hemi-brains of 9-month-old male mice. Representative confocal z-stack images of GFP-expressing neurons are shown on the left with genotypes as indicated. White arrow heads point to the dendritic spines. Scale bar, 5 µm. *Right*, quantification of spine density as shown on the left. Each dot represents one mouse (average of six dendrites). n=8–12. Data are represented by mean ± SEM. *, p<0.05, one-way ANOVA with Tukey's

Figure 7 continued on next page

Figure 7 continued

multiple comparisons test. (**B**) Representative volumetric MRI images in 6-month-old and 9-month-old male mice with genotypes as indicated. Arrow indicates enlargement of ventricles at 9 months of age compared with 6 months in P301S mice. (**C**) Longitudinal volumetric MRI quantification shows volume changes of ventricles, neocortex, and whole brain at 9 months of age compared with 6 months of age. Comparisons between all four genotypes at 9 months of age showed significant increase of ventricle volumes and decrease of neocortex and whole brain volumes in TauP301S mice and TPL-KD showed partial rescue of the TauP301S-dependent volume changes. n=11–12 male mice per genotype. Data are represented by mean ± SEM. *, p<0.05, **, p<0.01, ***, p<0.001, two-way ANOVA with Tukey's multiple comparisons test. (**D**) Quantification of plasma neurofilament light chain (NfL) levels from mice in (C). (**E**) Spontaneous locomotor activity of mice was evaluated in open field tests including total beam breaks, ambulatory bouts, and total rearings during a 20 min period. TauP301S mice showed hyperactivity, which was rescued by TPL2-KD. n=22–24 animals per genotype with male and female mice combined. *, p<0.05, **, p<0.01, ***, p<0.001, one-way ANOVA with Tukey's multiple comparisons test. (**F**) Memory of mice was evaluated using trace fear conditioning test. Percentage of time freezing during baseline recording time and during the trace interval time after the conditioned stimulus tone was compared for each genotype. n=10–12 animals per genotype. Data are represented by mean ± SEM. *, p<0.05, **, p<0.01, ***, p<0.001, two-way ANOVA with Bonferroni's multiple comparisons test.